Supporting Information

Regulating the Evaporation Surface Architecture of Anisotropic Chitosan Hydrogel for High-Efficiency Solar Desalination

Yuankun Wang[1], Defeng Wu[1,2*]

([1] School of Chemistry & Chemical Engineering, Yangzhou University, Yangzhou, Jiangsu Province, 225002, P. R. China)

([2] Provincial Key Laboratories of Environmental Materials & Engineering, Yangzhou, Jiangsu Province, 225002, P. R. China)

[*] Corresponding author. Tel.: +86 514 87975230; Fax: +86 514 87975244; E-mail address: dfwu@yzu.edu.cn.

Table Content

Video S1. Controlled nucleation in directional freezing step of (CC-He).

Video S2. Aligned growth of ice columns in the directional freezing step (CC-He).

Table S1. Structural parameters of the hydrogels (CC-Ho, CC-Di and CC-He) and the solar desalination performance of evaporators with different pore/vessel sizes

Evaporators	**CC-Ho**	**CC-Di**	**CC-He**
Surface morphology & Porous structure	Random 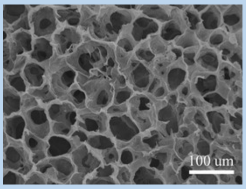	Anisotropic 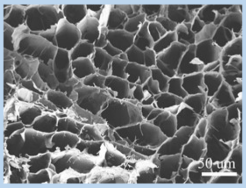	Radiant +Anisotropic 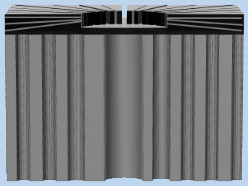
Pore/vessel size (μm)	60~80	Micro-channel: 30~40	Pit diameter: ~1000 Radiant vessel: ~25 Cellular channel: 30~50 Large-sized channel: 200~300
(3.5 wt%, 4 h, 1-sun) Rate (kg/m²·h)	2.23	3.18	3.86
Salt resistance	No	No	No
(20 wt%, 4 h, 1-sun) Rate (kg/m²·h)	1.52	2.98	3.82
Salt resistance	Yes	No	No
(20 wt%, 8 h, 2-sun) Rate (kg/m²·h)	None	3.09	5.14
Salt resistance		Yes	No
(20 wt%, 8 h, 3-sun) Rate (kg/m²·h)	None	2.92	6.55
Salt resistance		Yes	Salt shell

Table S2. The values of mechanical parameters f for the three types of hydrogels with or free of PA crosslinking

Samples	Young's modulus (KPa)	Yield strength (KPa)	Compression strength (KPa)
CC-Ho without PA	77.90±1.22	1.95±0.11	49.15±1.31
CC-Di without PA	119.38±1.70	2.94±0.22	37.16±1.07
CC-He without PA	72.14±0.61	2.50±0.13	58.11±1.18
CC-Ho	979.54±22.03	7.26±0.42	135.74±1.51
CC-Di	1013.70±3.50	18.93±0.21	117.61±1.35
CC-He	634.22±1.54	20.56±0.19	161.00±1.42

Table S3. Evaporation efficiencies of the CC-He hydrogel and some reported hydrogel-based evaporators

Hydrogel evaporators	**Morphology**	**Evaporation rate ($kg\ m^{-2}h^{-1}$)**	**Evaporation efficiency (%)**	**Conditions**
SPI/HEC/CB [*ref.*s1]	vertical radiant vessels	3.53	81.6	20 wt%/8h/1-sun
Cellulose/Alginate/CB [*ref.*s2]	3D-printed hierarchical porous	1.33	90.6	seawater/1h/1-sun
PVA/CS/PPy [*ref.*s3]	random porous	3.6	92	seawater/1h/1-sun
PVA/PPy [*ref.*s4]	micro-trees	3.64	96	seawater/1h/1-sun
PVA/KGM/Fe-MOF [*ref.*s5]	vertical tubular interconnected channels	3.2	90	seawater/1h/1-sun
Cellulose/CB [*ref.*s6]	monolithic design	1.82	95	seawater/1h/1-sun
PVA/SA/PAAS [*ref.*s7]	monolithic design	2.2	89.98	seawater/1h/1-sun
rGO/SA/PSF [*ref.*s8]	multi-channels	1.85	96.4	10 wt%/10h/1-sun
CS/CNT@TA (this work)	radial vessels and bimodal channels	3.87	96.7	20 wt%/8h/1-sun

[*ref.*s1] Liu, X.; Chen, F.; Li, Y.; Jiang, H.; Mishra, D. D.; Yu, F.; Chen, Z.; Hu, C.; Chen, Y.; Qu, L.; Zheng, W. 3D Hydrogel Evaporator with Vertical Radiant Vessels Breaking the Trade-Off between Thermal Localization and Salt Resistance for Solar Desalination of High-Salinity. Adv. Mater. 2022, 34 (36), 2203137.

[*ref.*s2] Yuan, J.; Lei, X.; Yi, C.; Jiang, H.; Liu, F.; Cheng, G. J. 3D-Printed Hierarchical Porous

Cellulose/Alginate/Carbon Black Hydrogel for High-Efficiency Solar Steam Generation. Chem. Eng. J. 2022, 430, 132765.

[*ref*.s3] Zhou, X.; Zhao, F.; Guo, Y.; Rosenberger, B.; Yu, G. Architecting Highly Hydratable Polymer Networks to Tune the Water State for Solar Water Purification. Sci. Adv. 2019, 5 (6), eaaw5484.

[*ref*.s4] Shi, Y.; Ilic, O.; Atwater, H. A.; Greer, J. R. All-Day Fresh Water Harvesting by Microstructured Hydrogel Membranes. Nat. Commun. 2021, 12 (1), 2797.

[*ref*.s5] Guo, Y.; Lu, H.; Zhao, F.; Zhou, X.; Shi, W.; Yu, G. Biomass-Derived Hybrid Hydrogel Evaporators for Cost-Effective Solar Water Purification. Adv. Mater. 2020, 32 (11), 1907061.

[*ref*.s6] Li, N.; Qiao, L.; He, J.; Wang, S.; Yu, L.; Murto, P.; Li, X.; Xu, X. Solar-Driven Interfacial Evaporation and Self-Powered Water Wave Detection Based on an All-Cellulose Monolithic Design. Adv. Funct. Mater. 2021, 31 (7), 2008681.

[*ref*.s7] Li, F.; Li, N.; Wang, S.; Qiao, L.; Yu, L.; Murto, P.; Xu, X. Self-Repairing and Damage-Tolerant Hydrogels for Efficient Solar-Powered Water Purification and Desalination. Adv. Funct. Mater. 2021, 31 (40), 2104464.

[*ref*.s8] Ma, H.; Yu, L.; Li, Z.; Chen, J.; Meng, J.; Song, Q.; Liu, Y.; Wang, Y.; Wu, Q.; Miao, M.; Zhi, C. A Lotus Seedpods-Inspired Interfacial Solar Steam Generator with Outstanding Salt Tolerance and Mechanical Properties for Efficient and Stable Seawater Desalination. Small 2023, 2304877.

Table S4. Ionic concentration variations before and after treatment

	Na^{+}(mg/L)	K^{+}(mg/L)	Ca^{2+}(mg/L)	Mg^{2+}(mg/L)
Before	14122.5	151.3	43.43	118.6
After	0.852	0.157	0.137	0.071

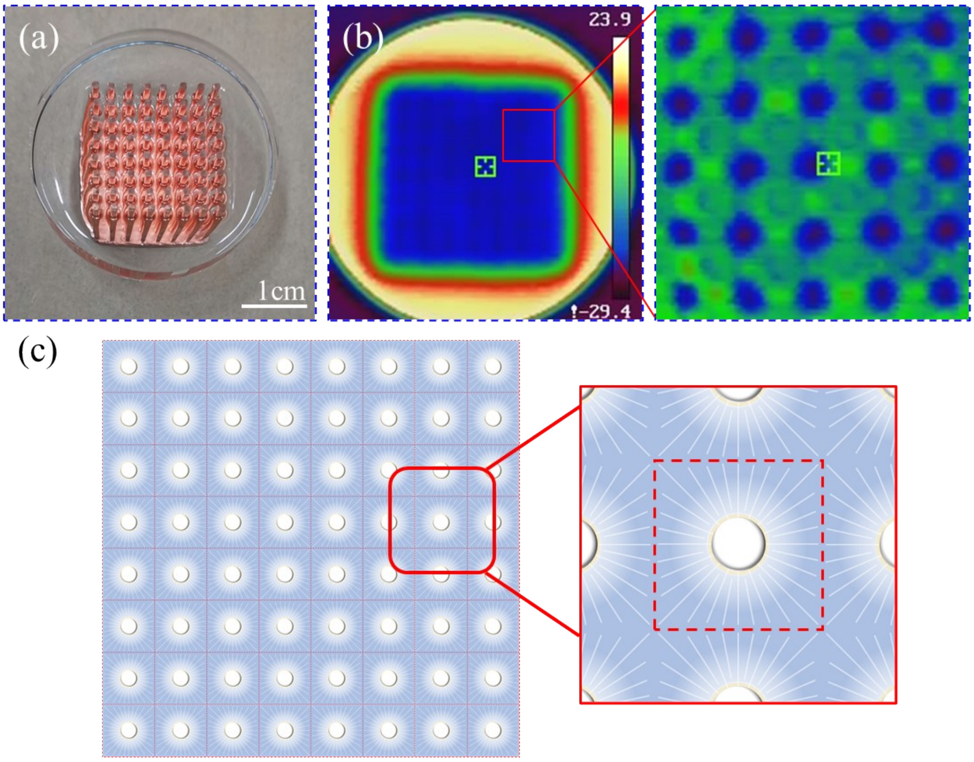

Figure S1. (a) The digital picture of the cold finger consisting of copper columns and PDMS, (b) the IR images showing uneven temperature distribution in a cold environment, and (c) the schematic diagram of heterogeneous nucleation.

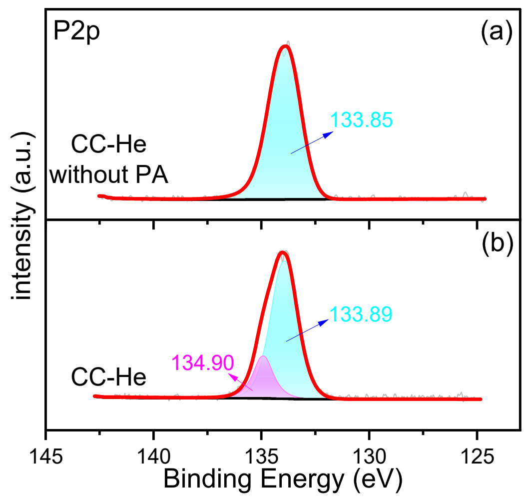

Figure S2. The P2p binding energy spectrum of (a) the CC-He hydrogel without PA treatment and (b) the CC-He hydrogel.

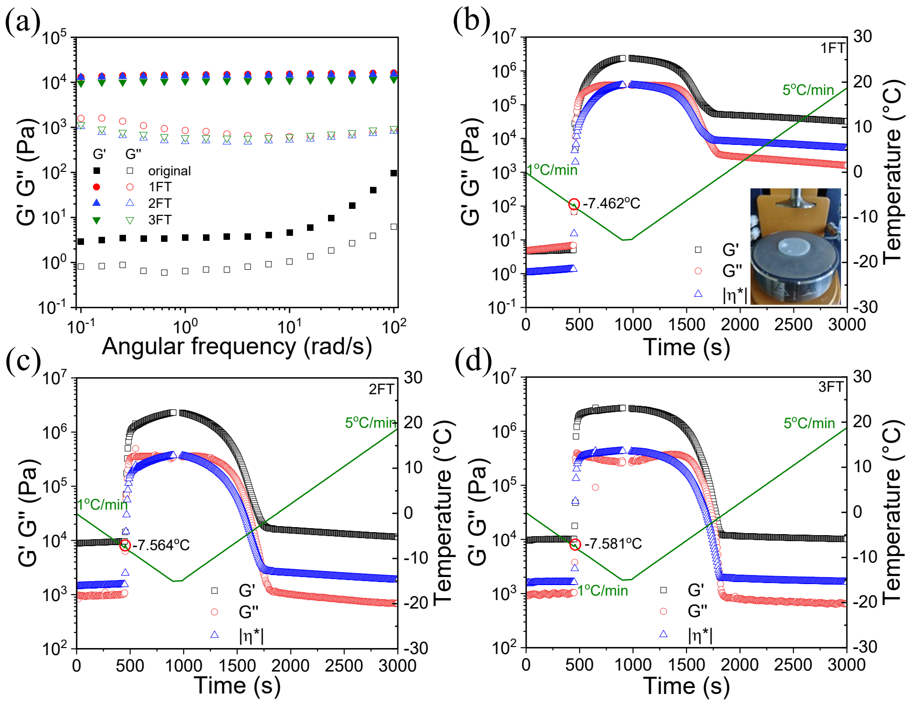

Figure S3. (a) The dynamic modulus alterations of the CS precursor after 3 cycles of freeze-thawing (FT) treatments, and (b-d) the modulus variations recorded during FT treatments.

Note: The freezing-thawing process was mimicked by the oscillation temperature ramp tests. The freezing rate (1 °C/min) was applied from 0 °C to -15 °C, then the temperature was raised to 25 °C with a heating rate (5 °C/min), and the modulus change was detected under 0.1% strain and 1 Hz. Then, the oscillation frequency sweep was immediately performed at 0.1% strain from 0.1 to 100 rad/s within the linear viscoelastic region. The freeze-thawing test was performed by 3 cycles. The results revealed that stable 3D physical networks could spontaneously form in the CS precursor under cold condition without additional freezing step.

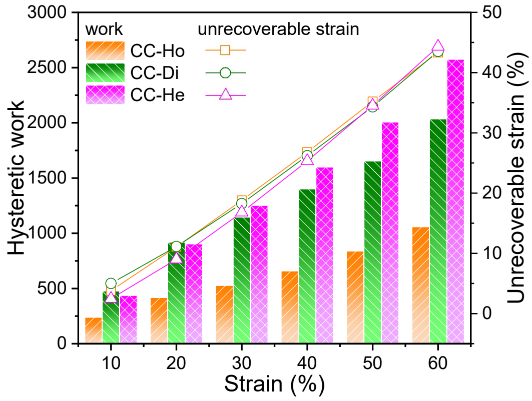

Figure S4. The integral area of hysteretic cycle and unrecoverable strain for each step of cyclic compression.

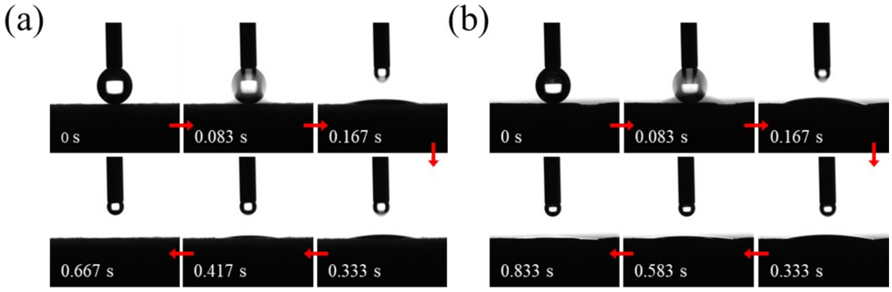

Figure S5. The absorption times of (a) CC-Di and (b) CC-Ho hydrogels.

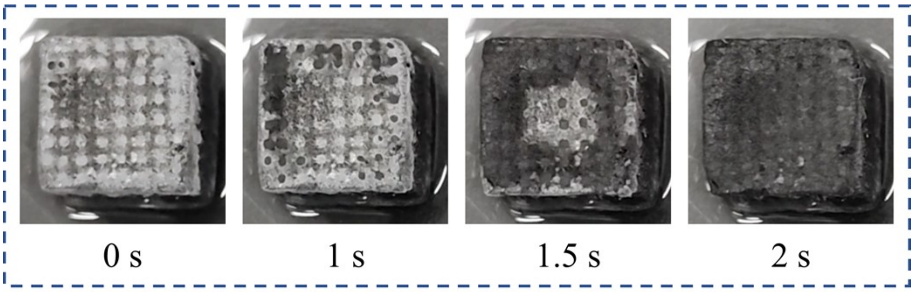

Figure S6. Top surface wetting process of the CC-He hydrogel through vertical water transportation.

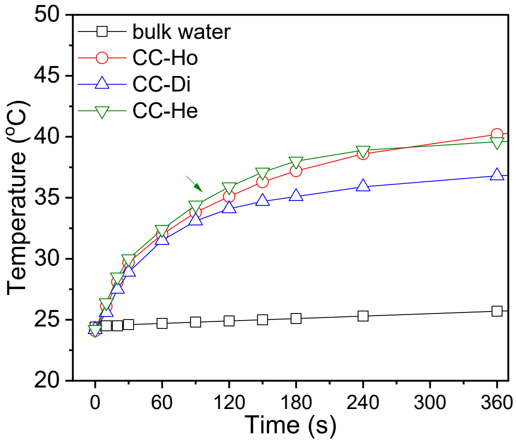

Figure S7. Surface temperature variations of bulk water, CC-Ho, CC-Di and CC-He evaporators under 1 sun illumination.

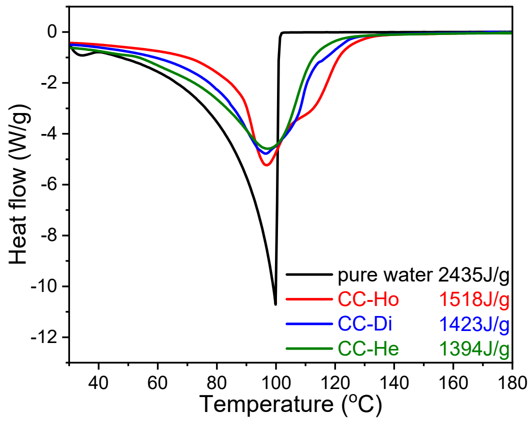

Figure S8. The DSC traces of pure water and the hydrogel evaporators with different structures (heating rate: 5 ^{o}C/min).

Note: The heat flow signal of pure water decreases dramatically after reaching the maximum at 100 ^{o}C, indicating that the water evaporation is completed immediately. The measured evaporation enthalpy of pure water is 2435 J/g, which is very close to the theoretical value of 2450 J/g. Due to the influence of polymer networks on the evaporation process, the evaporation enthalpy of water in the hydrogel evaporators is much small than that of pure water. However, the enthalpy values obtained by the DSC tests are higher than those tested in dark condition experiment because the DSC test presents a full dehydration that consumes additional energy for the bound water and free water in the hydrogels.

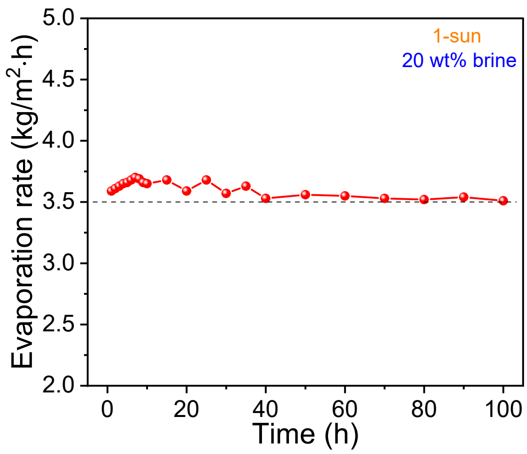

Figure S9. Long-term solar steam performance of the CC-He hydrogel under 1 sun for 100 h without salt blocking issue.

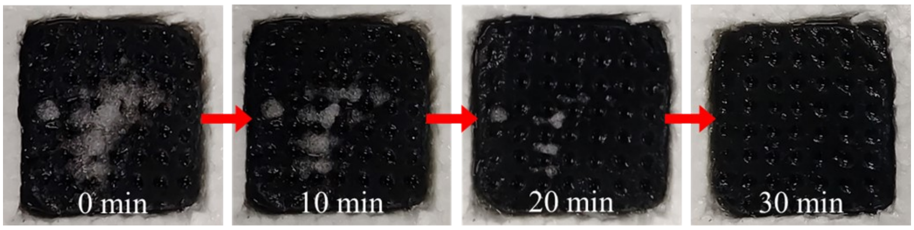

Figure S10. The digital pictures of the evaporation surface of CC-He preplaced with the salts (working in 20 wt% brine under 3-sun illumination).

Note: The salts preplaced on the evaporation surface of CC-He evaporator completely dissolved within 30 min (in 20 wt% brine) under 3-sun illumination. Dissolution occurred around the center (the radical paths and macro-pores coexist in this region), and then occurred away from the center gradually.